Evolution of Fiber Morphology During Electrospinning

Jian Fang, Hongxia Wang, Haitao Niu, Tong Lin, Xungai Wang

Centre for Material and Fibre Innovation, Deakin University, Geelong, Victoria 3217, Australia

Received 10 October 2009; accepted 25 March 2010
DOI 10.1002/app.32569
Published online 29 June 2010 in Wiley InterScience (www.interscience.wiley.com).

ABSTRACT: In this study, the morphological evolution of poly(acrylonitrile) (PAN) nanofibers during electrospinning was examined via immersion precipitation of newly electrospun filaments in ethanol, and subsequently associating the fiber morphologies with the electrospinning distances (2 to 10 cm). We have observed that an uneven fiber stretching happened throughout the electrospinning process. A massive filament-thinning took place at the initial stage of whipping instability, and fiber stretching at the later whipping stage was mainly concentrated on the bead sections, leading to improved uniformity of the resultant fibers. This work has provided a new insight into the fiber formation mechanism in the electrospinning process. © 2010 Wiley Periodicals, Inc. J Appl Polym Sci 118: 2553–2561, 2010

Key words: electrospinning; fiber morphology; immersion precipitation; polyacrylonitrile

INTRODUCTION

Electrospinning is a very useful technique to produce polymeric nanofibers for diverse applications.[1–7] This technique involves stretching a viscous polymer fluid under a strong electric field into fine filaments, which are typically deposited randomly on a grounded collector forming a nonwoven nanofiber mat. Improved electrospinning techniques have been able to produce bicomponent nanofibers,[8–11] aligned fiber array,[12–15] fibers with a porous surface[16,17] or other novel fibrous structures.[18–20]

The fiber stretching in electrospinning is a fast and incessant process, which can be divided into three consecutive stages[1,3]: jet initiation, whipping instability, and fiber deposition. From the initial jet to dry fibers, the fiber stretching process takes place in milliseconds.[21] Although extensive works have been undertaken to understand the effects of operating parameters (e.g., applied voltage, spinning distance, flow rate of polymer solution) and initial material properties (e.g., solution viscosity, conductivity, surface tension, solvent volatility) on the electrospinning process and resultant fiber morphology,[22–26] little is known on how the jet/filament changes its morphology during electrospinning. As a result of lacking in-depth understanding of the fiber stretching mechanism, the control of electrospinning process and fiber morphology has been based on adjusting the operating parameters and initial solution properties.

In previous studies,[21,27–29] a high-speed video camera combined with a long distance optical microscopic lens was used to observe an electrospinning process, and a single-fiber stretching mechanism accompanied with a helical whipping movement was observed. However, the relatively low resolution of optical microscope system made it impossible to trace the filament morphology change during electrospinning due to the small filament diameter.

In fiber and membrane industries, immersion precipitation has been a commonly used principle for producing porous membranes or wet-spun fibers.[30,31] Using a nonsolvent as coagulant, a polymer solution can be solidified rapidly into desired shapes. The process and resultant polymer morphology are controlled by diffusion kinetics of solvent and nonsolvent.

In this study, we have used, for the first time, the immersion precipitation method to rapidly solidify newly electrospun PAN filaments at different spinning distances, so that the fiber morphology evolution in electrospinning can be established indirectly. The reason for not using normal electrode collector to collect as-spun nanofibers is that liquid filament cannot maintain their morphology when the collection distance is short.[32,33]

EXPERIMENTAL

Materials and measurements

Polyacrylonitrile (M_w = 86,200 g/mol), *N*,*N*-dimethylformamide (DMF) and ethanol were obtained from

Correspondence to: T. Lin (tongl@deakin.edu.au).
Contract grant sponsor: Australian Research Council under Discovery Grant scheme; contract grant number: ARC DP0985364.
Contract grant sponsor: Deakin University under the Central Research Grant Scheme.

Aldrich and used as received. The fiber morphology was observed under a scanning electron microscope (SEM, LEO 1530 microscope). The fiber morphologies (fiber diameter, bead size) were analyzed based on the SEM images with the aid of an image analysis software (Image*Pro+6.0*). At least 200 fibers were counted in each calculation.

Cloud point data were obtained by titration method. Mixed solvent and nonsolvent (1 : 1 in volume) were slowly added to a homogeneous polymer solution using a syringe at room temperature. The cloud point was calculated when the solution remained turbid for more than 24 h.

The immersion precipitation kinetics of PAN-DMF solutions in ethanol was measured by light transmittance method.[30] The measurement was performed using an optical-fiber UV-visible spectroscope system including a vertically set cuvette holder, a UV-VIS-NIR light source (DH-2000-BAL) and a UV-VIS spectrometer (USB 4000). The system is controlled by a personal computer with software (SpectraSuite). In the measurement, a film (~300 μm in thickness) of PAN solution on quartz plate was immersed instantly into the ethanol, and *real-time* light transmittance of the solution film was recorded. Many previous researches[34,35] have proven the coagulation speed can be denoted as $\xi/\sqrt{t}$, where ξ is the thickness of solidified liquid layer during the coagulation process and t presents coagulation time. The coagulation speed of the solution film in this research was calculated according to eq. (1):

$$\text{Coagulation speed} = \text{film thickness}/\sqrt{\text{complete coagulation time}}. \quad (1)$$

The electric field strength was calculated with a finite element method using the software Femlab3.4. In the subdomain settings, the constitutive relation $D = \varepsilon_0\varepsilon_r$ was used together with $E = -\nabla V$ to obtain the equation below,

$$-\nabla \cdot \varepsilon_0\varepsilon_r\nabla V = \rho, \quad (2)$$

where E is the electric field strength, ε_r is the relative permittivity which is 1 for air and 24.3 for ethanol,[36] and ρ is the space charge density. During boundary setting, only the needle was set under applied potential and electric potentials of other boundaries were all set as zero.

Electrospinning

A purpose-built electrospinning apparatus was used in this work (Fig. 1). The polymer solution was put into a 5 mL plastic syringe and connected to a high voltage power supply (ES30P, Gamma High Voltage Research) via a metal syringe needle (21 Gauge). A round copper disk (diameter = 8 cm), used as the grounded electrode, was placed in a plastic flask (inner diameter = 9 cm and depth = 15 cm) right underneath the syringe needle (nozzle). The distance between the tip of the nozzle and the copper disk was fixed at 15 cm. Before electrospinning, ethanol was added into the plastic flask so that the as-spun fibers were directly electrospun into the ethanol bath before reaching the grounded electrode, and the distance between the nozzle tip and ethanol surface (d) was changed via adjusting the volume of ethanol. During electrospinning, the flow rate of the PAN solution was controlled at 1.0 mL/h using a digital syringe pump (KD scientific). The distance between the needle tip and ethanol surface was set in the range of 2–10 cm.

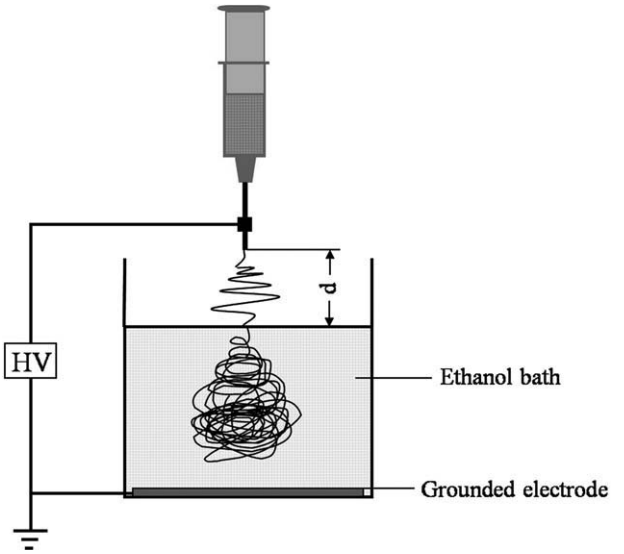

Figure 1 Apparatus for solidifying the newly electrospun fibers at different distances.

RESULTS AND DISCUSSION

Figure 1 shows the apparatus for *in-situ* solidification of the newly electrospun fibers at different electrospinning distances. The liquid filaments were directly deposited into an ethanol bath set between the nozzle and the grounded electrode during electrospinning. Once the filaments came into contact with the ethanol, immersion precipitation occurred immediately, resulting in solid filaments that were easily observed under SEM.

The key to trace the fiber morphology evolution using the immersion precipitation method is to ensure that no morphology contrast occurs during the process. To verify this, the phase separation behavior of the PAN-DMF-ethanol ternary system and the kinetics of immersing PAN-DMF solution in ethanol were examined.

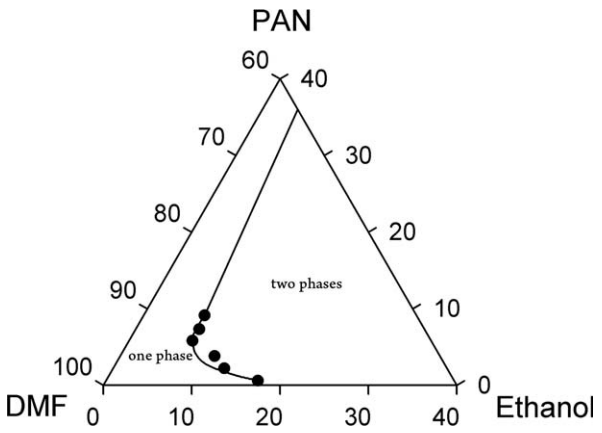

Figure 2 Cloud points in the system consisting of PAN, DMF, and ethanol.

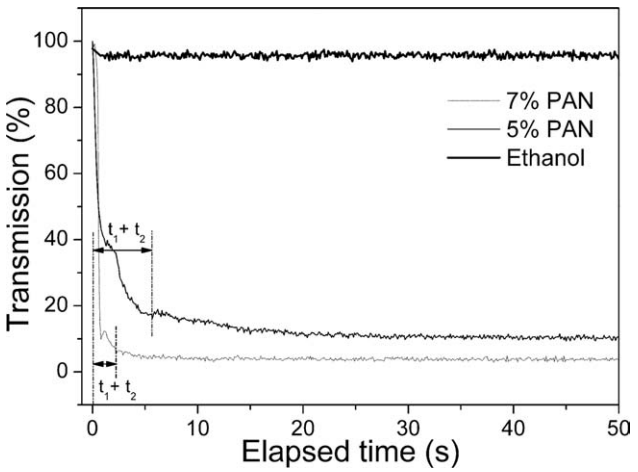

Figure 3 Light transmittance curves of PAN solution membranes in ethanol.

The cloud point curve phase diagram, which shows the critical composition of ternary system from thermodynamically stable to unstable states,[37] for the PAN-DMF-ethanol mixture at room temperature was measured by the turbidity method and shown in Figure 2. The ethanol concentration varied from 6.9 to 17.2% when the PAN concentration changed from 11 to 1%. The phase diagram shown in Figure 2 reveals small liquid–liquid de-mixing region and a typical instantaneous de-mixing tendency for the PAN-DMF-ethanol system,[38] which is ideal for instant solidification of PAN-DMF filaments. Such an instant solidification is the key to ensure the filaments maintaining their original morphology during the collection in electrospinning.

In kinetics, an immersion precipitation is a nonequilibrium process involving liquid–liquid de-mixing and gelation driven by diffusion of solvent and nonsolvent between the polymer solution and nonsolvent. Phase separation occurs during the process, leading to apparent reduction in the light transmittance. The kinetics of an immersion precipitation process can be examined by measuring the change of light transmittance of a solution film with the coagulation time. A typical light transmittance $\sim$ time curve includes three specific time periods[39]: delayed time (t_1), de-mixing time (t_2), and time of final solidification (t_3). The delayed time is usually very short. For an instantaneous de-mixing, $t_1 = 0$. The de-mixing time is determined by the mutual diffusion between solvent and nonsolvent and also the viscosity of polymer system. The t_3 is the time for the de-mixed film to be solidified completely. The t_2 and t_3 are also dependent on the thickness of the polymer solution film. In such a kinetic process, the rate of polymer precipitation, also called coagulation rate, plays a dominant role in maintaining the morphology of the solidified polymer filaments.

Inside the nonsolvent, removal of solvent from the coagulating filament and the solidification of dissolved polymer take place simultaneously. The solid skin starts to form on the filament surface, and the solidification then moves inwards the filament. If the skin layer is rigid and the solidification experiences

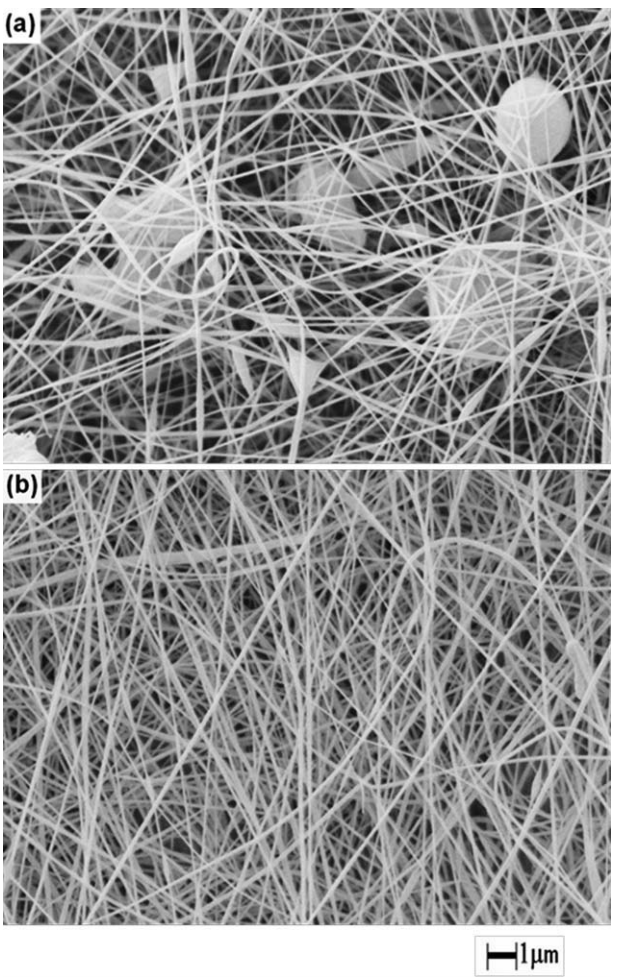

Figure 4 SEM images of PAN nanofibers electrospun from (a) 5 and (b) 7 wt % PAN/DMF solutions (Applied voltage = 18 kV and spinning distance = 15 cm).

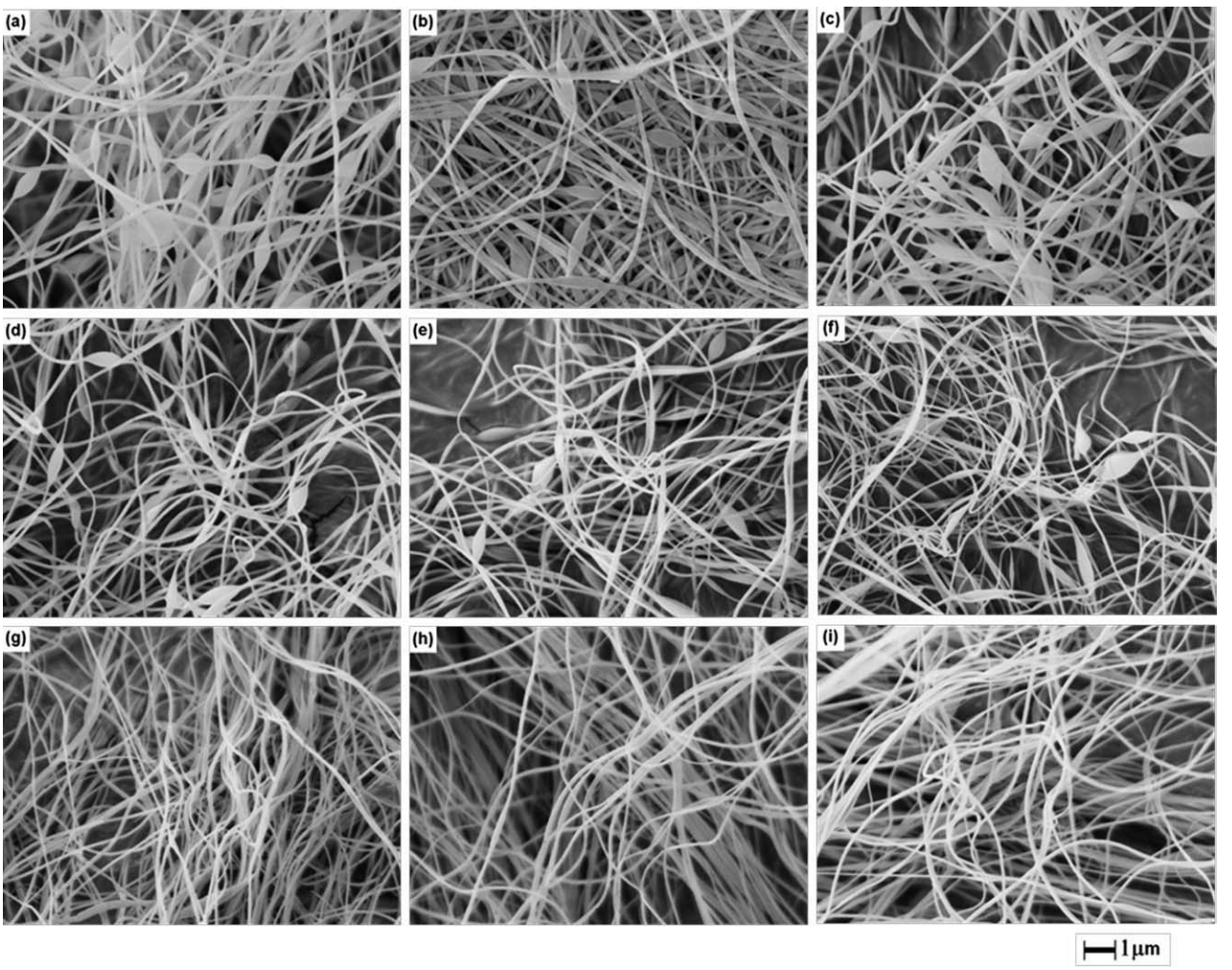

Figure 5 SEM images of electrospun PAN nanofibers at different collecting distances; (a) 2 cm, (b) 3 cm, (c) 4 cm, (d) 5 cm, (e) 6 cm, (f) 7 cm, (g) 8 cm, (h) 9 cm, and (i) 10 cm (PAN concentration = 7 wt %, applied voltage = 18 kV).

a large volume change, deformation in filament cross section could happen. However, such a morphology contrast can be overcome if the coagulation rate is high enough. A higher coagulation rate provides a shorter solidification time, thus the chance for filaments to get deformed is limited.

Figure 3 shows the light transmittance $\sim$ time curves of cast PAN-DMF solution films in ethanol. A very small $t_1 + t_2$ indicated an instantaneous liquid–liquid de-mixing happening in the processes. Based on the curves, the coagulation rates were calculated, to be 10^{-4} m/sec$^{1/2}$ and 6×10^{-5} m/sec$^{1/2}$ for the 7 and 5 wt % PAN solutions, respectively. Based on this data and dimension of liquid solution, the time required to solidify a PAN-DMF solution filament can be estimated.

In our case, two PAN/DMF solutions of concentration 5 and 7 wt % were electrospun into nanofibers. When the 5 wt % PAN solution was electrospun using a normal electrospinning apparatus,[23] fibers with a beads-on-string structure and diameter of 120 $\pm$ 21 nm were produced, as shown in Figure 4. Electrospinning 7 wt % PAN solution under the same operating condition resulted in bead-free and uniform fibers (diameter = 197 $\pm$ 21 nm). Based on the fiber diameter and the concentration of PAN in the solution, one can estimate that producing a PAN fiber of 120 nm in diameter from 5 wt % PAN solution will require a liquid filament of diameter up to 540 nm if the spinning process is not considered. Using the above calculated coagulation rate, it can be estimated that complete coagulation of a liquid film of the thickness equivalent to the liquid filament diameter (540 nm) in ethanol will take $\sim$ 0.06 milliseconds. Even if the liquid film is ten times thicker, the coagulation process is still very fast (less than 6.4 milliseconds). For the liquid filaments, the solidification should be much faster than that of the liquid film because the diffusion can take place in different directions. With the 7 wt % PAN solution, the filament solidification should be faster compared with

that from the 5 wt % solution because of higher coagulation rate.

It should be noted that the above estimation is on the base of that the PAN concentration does not change before the solution filament contacts with ethanol. Since the solvent rapidly evaporates from the filaments during the electrospinning process, the increased PAN concentration would also speed up the solidification process. These results suggested that the morphology contrast during the solidification of the newly electrospun PAN-DMF filaments in ethanol should be less likely to happen.

When the PAN solution was directly electrospun into the ethanol solution using the apparatus shown in Figure 1, fibers collected at different collecting distances had different morphologies. Figure 5 shows the SEM images of the PAN fibers electrospun from 7 wt % PAN solution solidified at 2–10 cm away from the nozzle tip. With the increase in collecting distance, the beaded fibers were always produced until the collecting distance exceeded 7 cm [Fig. 5(a–f)]. Longer collecting distance led to bead-free fibers [Fig. 5(g–i)].

The average fiber diameter calculated based on the string sections varied with the collecting distance. As shown in Figure 6(a), the fibers collected at the spinning distance of 2 cm have a diameter of 220 ± 30 nm. When the spinning distance was increased from 2 to 4 cm, the fiber diameter maintained at the same level, but the diameter distribution became narrowed. When the collecting distance was further increased, the fiber diameter reduced slightly. The fitting curve in the figure can clearly show the decreasing trend of fiber diameter and increasing the collecting distance from 2 to 10 cm only led to about 30 nm reduction in the average fiber diameter.

Using a long distance microscope, the dimensions of the "Taylor cone" and the subsequent stable-jet were measured. The length of the "Taylor cone" was 2–3 mm, and the length and diameter of the stable-jet were around 6–10 mm and 200 μm, respectively. The diameter of dried jet estimated from the liquid jet diameter and initial polymer concentration (7 wt %) was about 53 μm. After the stable-jet, from 1.3–2.0 cm, the fiber diameter changed from around 50 μm to 220 nm. This result suggested that rapid jet/filament stretching occurred at the initial stage of the whipping instability.

Also, the fiber beads changed their dimension with the collecting distance. As shown in Figure 6(b), large beads with the width and length of 960 ± 0.27 nm and 2.72 ± 0.39 μm, respectively, were collected at 2 cm away from the nozzle tip. With the collecting distance increasing from 2 to 7 cm, the changes in bead width and length were within the scale of error bar. When the collecting distance was longer than 7 cm, no beads were found among the

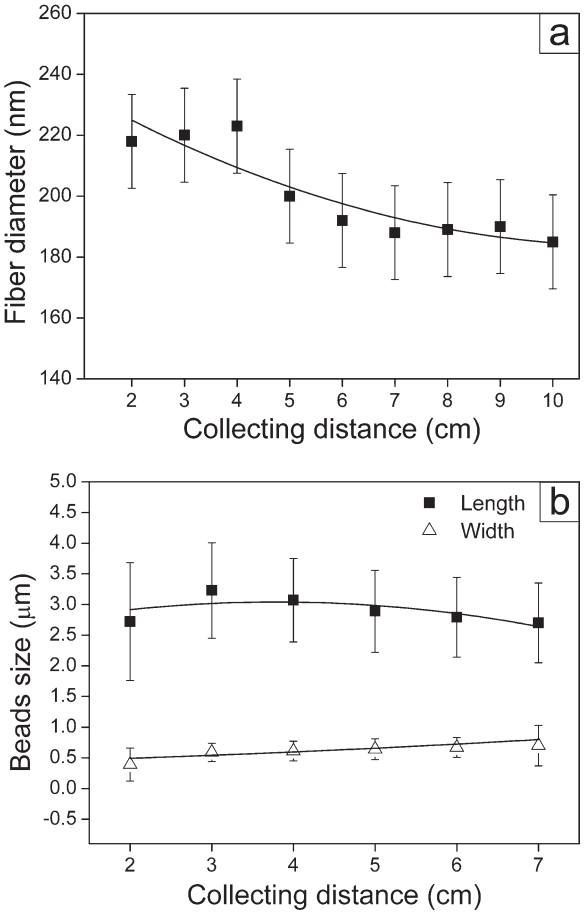

Figure 6 Average fiber diameter (a) and bead dimension (b) of PAN fibers at different collecting distances (PAN concentration = 7 wt %).

fibers collected, indicating that the beads were elongated into uniform fibers at the later stage of whipping instability.

When the 5 wt % PAN/DMF solution was electrospun, beads-on-string fibers were produced even when the collecting distance was as long as 10 cm (Fig. 7). The fiber diameter reduced gradually from 150 ± 25 nm to 105 ± 25 nm when the collecting distance increased from 2 to 10 cm [Fig. 8(a)]. Also, with the increase in the collecting distance, the bead width changed little, and the bead length reduced slightly at the longer collecting distances [Fig. 8(b)].

In comparison to the fibers electrospun from 7 wt % PAN solution, the fibers electrospun from 5 wt % PAN solution have smaller string diameter and bead size on average. When the collecting distance was larger than 7 cm, beaded fibers were still produced from the 5 wt % PAN solution.

The introduction of a dielectric substance into an electrical field could change the electrical field intensity. Since the jet instability comes from the interaction between the charged jet and the external electrical field and electrostatic repulsion within the

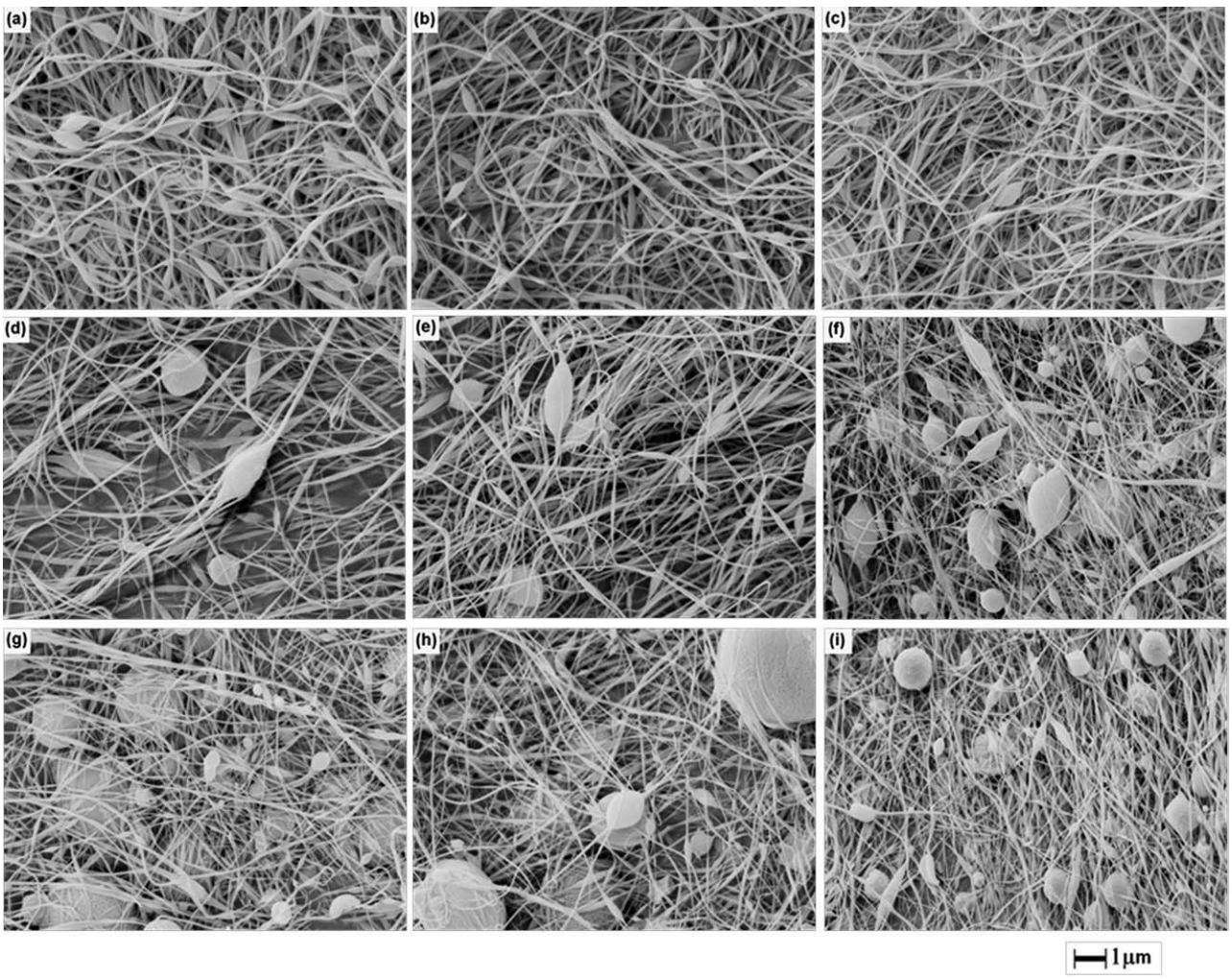

Figure 7 SEM images of electrospun PAN nanofibers at different collecting distances; (a) 2 cm, (b) 3 cm, (c) 4 cm, (d) 5 cm, (e) 6 cm, (f) 7 cm, (g) 8 cm, (h) 9 cm, and (i) 10 cm (PAN concentration = 5 wt %, applied voltage = 18 kV).

jet,[23,29,40] the effect of ethanol bath on the external electrical field must be considered. The electric field intensity along the direction from the nozzle to the grounded electrode was obtained through a finite element analysis. As shown in Figure 9(a), under a constant applied voltage (18 kV), the intensity of electric field decayed rapidly within the first 1.5 cm away from the nozzle, and the rate of decay slowed down considerably afterwards. However, once an ethanol bath was placed between the nozzle and the grounded electrode, the electric field intensity in the ethanol bath reduced to zero rapidly. The electric field intensity in the area from nozzle tip to the liquid surface of the ethanol bath was increased. Also, the height of ethanol bath affected the electric field strength. A higher ethanol bath, corresponding to shorter spinning distance d, led to higher electric field strength. The filaments under a higher electric force would be stretched thinner than that electrospun without ethanol involved in the fiber collection process.

To eliminate the influence arising from the ethanol bath, the applied voltage was adjusted so that the electric field strength had an equivalent profile to that without the ethanol. With different ethanol heights, the applied voltage used to generate the fitted electric field profiles varied, and a higher ethanol bath needed a lower applied voltage to achieve the required electric field profile [Fig. 9(b)].

Under the adjusted voltages [Fig. 9(b)], both PAN solutions were electrospun at different collecting distances once again, with other operating parameters remaining unchanged. It was found that fiber diameter decreased dramatically from 200 μm to hundreds of nanometers (320 nm from 7 wt % solution and 200 nm from 5 wt % solution) at a very short spinning distance (<2 cm), and beaded fibers were still obtained from 7 wt % PAN solution when the spinning distance was in the range of 2–6 cm, while the fibers became bead-free and uniform when the collecting distance was greater than 7 cm. For fibers electrospun from the 5 wt % solution, large fiber

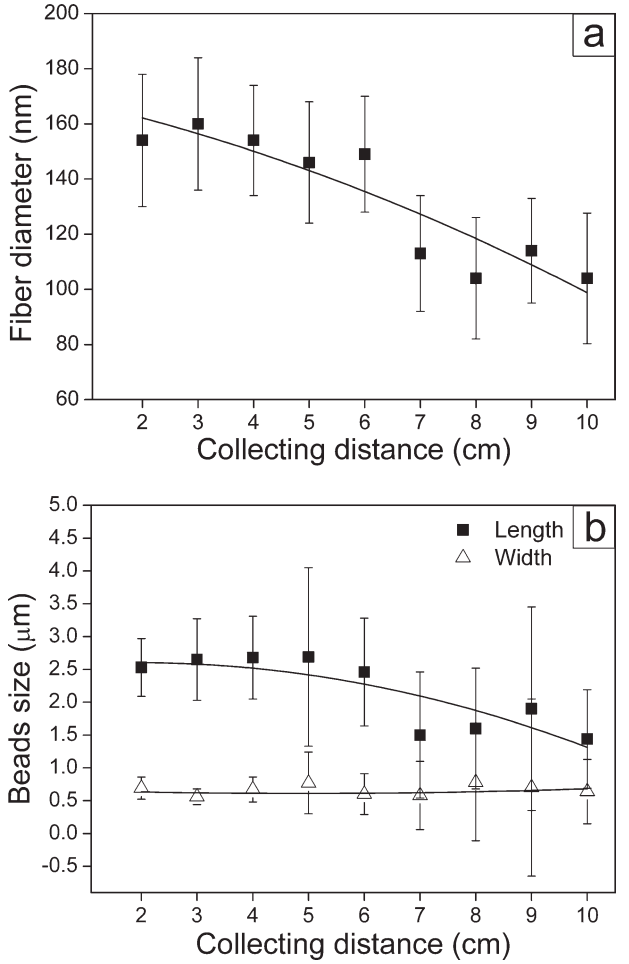

Figure 8 Average fiber diameter (a) and bead dimension (b) of PAN fibers at different collecting distances (PAN concentration = 5 wt %).

diameter reduction was also found at the early whipping stage. However, beads on the fibers did not disappear even when the collecting distance was long. As a result of reducing the applied voltages, electrostatic interactions between the charged filaments and the electric field were reduced, and both fibers and beads became coarser than those that were electrospun under a constant applied voltage.

Bead density on nanofibers was counted and shown in Figure 10. It was noted that the bead density decreased gradually with the increase in the electrospinning distance for the nanofibers electrospun from the 7 wt % PAN solution, regardless whether the electrospinning was operated under the same applied voltage or the same electric field strength. This suggested that beads were gradually eliminated over the electrospinning distance, which is the main reason to form bead-free nanofibers. Although the beads in the nanofibers electrospun from 5 wt % solution showed a similar trend in the size change, they were not eliminated, presumably because the filaments contained a high concentration of solvent and the fiber stretching force was relatively weak at the later stage of the whipping.

Based on the fiber and bead dimensions listed in Figures 6 and 8, the fiber morphology evolution in electrospinning the two PAN solutions can be summarized in Figure 11. No matter whether the electrospinning process was conducted under the same applied voltage or the same electric field strength, fiber morphology changes followed a similar trend. For the 7 wt % PAN solution, beaded fibers were collected until the collecting distance was longer than 7 cm. Longer collecting distance led to bead-free uniform fibers. For the 5 wt % PAN solution, although beaded fibers were collected at a short distance, longer electrospinning distance still resulted in the beads-on-string structure. Regardless the morphology evolutions, the uniform fibers electrospun from 7 wt % PAN solution and the beaded fibers from 5 wt % are in accordance with the electrospinning results without using ethanol bath as collector

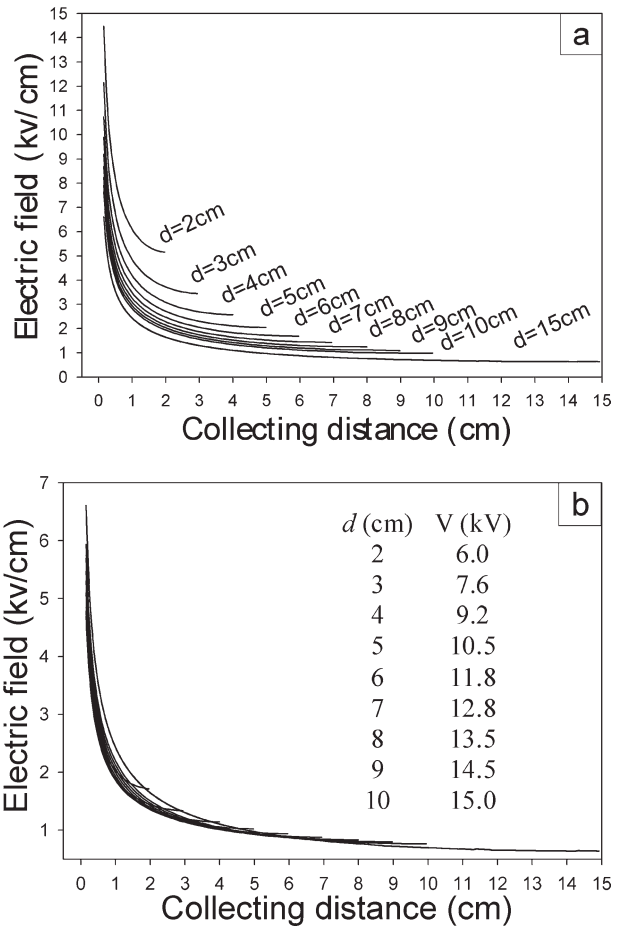

Figure 9 (a) Calculated electric field strength along the electrospinning area. Nozzle tip (distance = 0), grounded electrode (distance = 15). The *d* is the distance between the tip of nozzle and the ethanol liquid surface (Applied voltage = 18 kV); (b) Recalculated electric field strength based on the adjusted applied voltage.

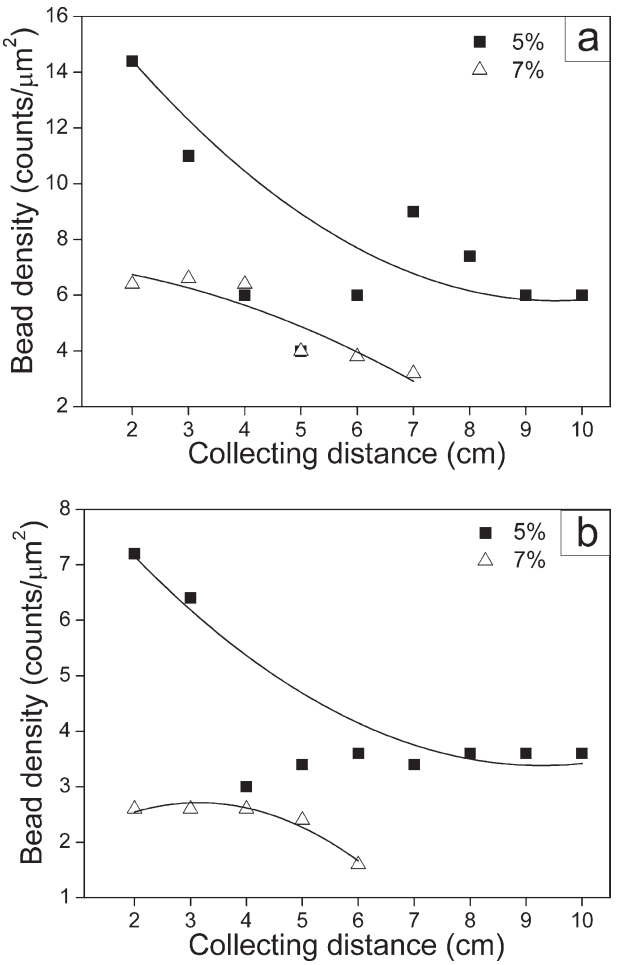

Figure 10 Bead density on PAN fibers at different collecting distances under (a) constant applied voltage and (b) adjusted applied voltage.

(Fig. 4). Electrospinning other polymers, such as polystyrene, showed a similar trend in morphology change during electrospinning.

CONCLUSIONS

In this research, we have used an immersion precipitation process that can rapidly solidify polymer filaments to evaluate fiber morphology changes in an electrospinning process. By collecting the newly electrospun PAN fibers at different electrospinning distances, the evolution of fiber morphologies during electrospinning has been established. It was revealed that a massive jet thinning and associated fiber diameter reduction took place at the initial stage of the whipping instability. The fiber stretching at the later stage of whipping was mainly concentrated on the beaded sections, which improves the overall fiber uniformity. Although the dimension of fibers electrospun under constant applied voltages and constant electric filed strength varied, the fiber morphology change along the electrospinning distance followed a similar trend. The results suggest that enhancing

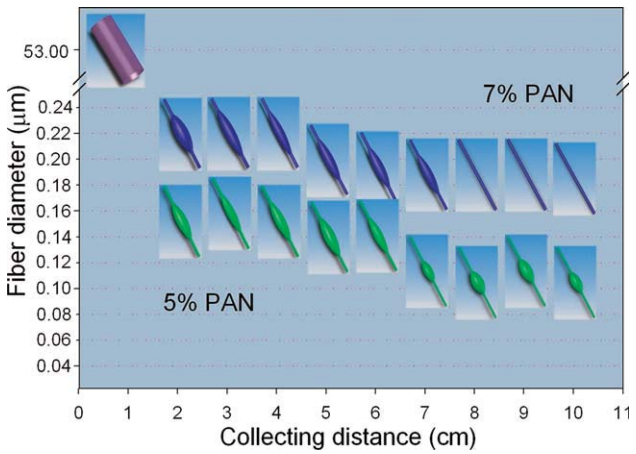

Figure 11 The evolution of fibers in electrospinning two PAN solutions, the fiber, and bead dimensions were obtained from data shown in Figures 6 and 8. [Color figure can be viewed in the online issue, which is available at www.interscience.wiley.com.]

fiber drawing at the initial stage of whipping will be an efficient way to obtain finer nanofibers, and enhancing fiber stretching at the later stage of whipping improves fiber uniformity.

References

1. Subbiah, T.; Bhat, G. S.; Tock, R. W.; Parameswaran, S.; Ramkumar, S. S. J Appl Polym Sci 2005, 96, 557.
2. Teo, W. E.; Ramakrishna, S. Nanotechnology 2006, 17, R89.
3. Dzenis, Y. Science 2004, 304, 1917.
4. Abidian, M. R.; Kim, D.-H.; Martin, D. C. Adv Mater 2006, 18, 405.
5. Bhattarai, S. R.; Bhattarai, N.; Yi, H. K.; Hwang, P. H.; Cha, D. I.; Kim, H. Y. Biomaterials 2004, 25, 2595.
6. Wang, X.; Drew, C.; Lee, S.-H.; Senecal, K. J.; Kumar, J.; Samuelson, L. A. J Macromol Sci 2002, 39, 1251.
7. McCann, J. T.; Marquez, M.; Xia, Y. J Am Chem Soc 2006, 128, 1436.
8. McCann, J. T.; Li, D.; Xia, Y. J Mater Chem 2005, 15, 735.
9. Wei, M.; Kang, B.; Sung, C.; Mead, J. Macromol Mater Eng 2006, 291, 1307.
10. McCann Jesse, T.; Marquez, M.; Xia, Y. Nano Lett 2006, 6, 2868.
11. Lin, T.; Wang, H.; Wang, X. Adv Mater 2005, 17, 2699.
12. Li, D.; Ouyang, G.; McCann, J. T.; Xia, Y. Nano Lett 2005, 5, 913.
13. Zhong, S.; Teo, W. E.; Zhu, X.; Beuerman, R. W.; Ramakrishna, S.; Yung, L. Y. L. J Biomed Mater Res Part A 2006, 79, 456.
14. Katta, P.; Alessandro, M.; Ramsier, R. D.; Chase, G. G. Nano Lett 2004, 4, 2215.
15. Teo, W. E.; Ramakrishna, S. Nanotechnology 2005, 16, 1878.
16. Dosunmu, O. O.; Chase, G. G.; Kataphinan, W.; Reneker, D. H. Nanotechnology 2006, 17, 1123.
17. Patel, A. C.; Li, S.; Yuan, J.-M.; Wei, Y. Nano Lett 2006, 6, 1042.
18. Smit, E.; Buttner, U.; Sanderson, R. D. Polymer 2005, 46, 2419.
19. Pan, H.; Li, L.; Hu, L.; Cui, X. Polymer 2006, 47, 4901.
20. Stitzel, J.; Liu, J.; Lee Sang, J.; Komura, M.; Berry, J.; Soker, S.; Lim, G.; Van Dyke, M.; Czerw, R.; Yoo James, J.; Atala, A. Biomaterials 2006, 27, 1088.
21. Reneker, D. H.; Yarin, A. L.; Fong, H.; Koombhongse, S. J Appl Phys 2000, 87, 4531.

22. Lin, T.; Fang, J.; Wang, H.; Cheng, T.; Wang, X. Nanotechnology 2006, 17, 3718.
23. Lin, T.; Wang, H.; Wang, H.; Wang, X. Nanotechnology 2004, 15, 1375.
24. Mit-Uppatham, C.; Nithitanakul, M.; Supaphol, P. Macromol Chem Phys 2004, 205, 2327.
25. Theron, S. A.; Zussman, E.; Yarin, A. L. Polymer 2004, 45, 2017.
26. Deitzel, J. M.; Kleinmeyer, J.; Harris, D.; Beck Tan, N. C. Polymer 2001, 42, 261.
27. Shin, Y. M.; Hohman, M. M.; Brenner, M. P.; Rutledge, G. C. Polymer 2001, 42, 9955.
28. Hohman, M. M.; Shin, M.; Rutledge, G.; Brenner, M. P. Phys Fluids 2001, 13, 2221.
29. Yarin, A. L.; Koombhongse, S.; Reneker, D. H. J Appl Phys 2001, 89, 3018.
30. Mulder, M. Basic Principles of Membrane Technology; 2nd ed.; Kluwer Academic Publishers: Dordrecht, The Netherlands, 1996.
31. Andrzej, Z. Fundamentals of Fibre Formation: The Science of Fibre Spinning and Drawing, John Wiley & Sons Ltd: London, 1976.
32. Buchko, C. J.; Chen, L. C.; Shen, Y.; Martin, D. C. Polymer 1999, 40, 7397.
33. Kameoka, J.; Orth, R.; Yang, Y.; Czaplewski, D.; Mathers, R.; Coates, G. W.; Craighead, H. G. Nanotechnology 2003, 14, 1124.
34. Paul, D. R. J Appl Polym Sci 1968, 12, 383.
35. Ji, B. H.; Wang, J. H.; Wang, C. G.; Wang, Y. X. J Appl Polym Sci 2008, 108, 328.
36. Somasundaran, P. Encyclopedia of Surface and Colloid Science; CRC Press: Florida, 2006.
37. Zhu, L.; Zhu, B.; Xu, Y. J Appl Polym Sci 2006, 101, 878.
38. Machado, P. S. T.; Habert, A. C.; Borges, C. P. J Membr Sci 1999, 155, 171.
39. Um, I. C.; Kweon, H.; Lee, K. G.; Ihm, D. W.; Lee, J.-H.; Park, Y. H. Int J Biol Macromol 2004, 34, 89.
40. Hohman, M. M.; Shin, M.; Rutledge, G.; Brenner, M. P. Phys Fluids 2001, 13, 2201.